AD-A090 571 WYOMING UNIV LARAMIE DEPT OF MECHANICAL ENGINEERING F/G 11/4
DAMAGE MECHANISMS/FAILURE MECHANICS OF CARBON-CARBON COMPOSITE --ETC(U)
SEP 79 D E WALRATH, D F ADAMS N00014-77-C-0503
UNCLASSIFIED UWME-DR-904-101-1 NL

1 OF 1
AD A090571

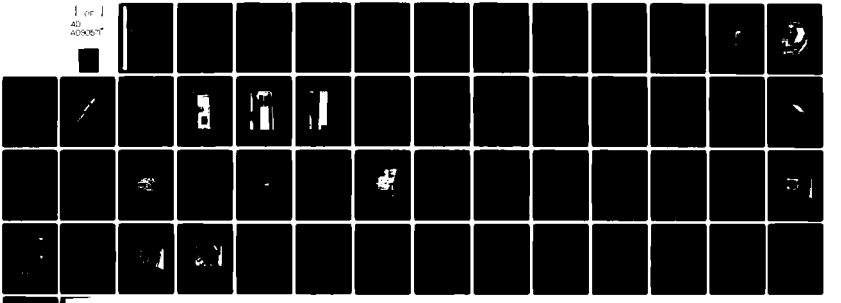

END
DATE FILMED
11-80
DTIC

UWME-DR-904-101-1

DAMAGE MECHANISMS/ FAILURE MECHANICS OF CARBON-CARBON COMPOSITE MATERIALS

David E. Walrath
Donald F. Adams

September 1979

INTERIM REPORT
Office of Naval Research
Grant No. NOOO 14-77-C-0503

COMPOSITE MATERIALS RESEARCH GROUP
DEPARTMENT of MECHANICAL ENGINEERING
University of Wyoming Laramie, Wyoming 82071

DAMAGE MECHANISMS / FAILURE MECHANICS OF CARBON-CARBON COMPOSITE MATERIALS

Interim Report

UWME-DR-904-101-1

September 1979

Submitted to:

Office of Naval Research
Arlington, Virginia 22217

Attention: Dr. Arthur M. Diness, Director
Metallurgy and Ceramics Program

ONR Contract N00014-77-C-0503
Project No. NR 039-149/5-18-77 (471)

Submitted by:

David E. Walrath and Donald F. Adams
Principal Investigators
Department of Mechanical Engineering
University of Wyoming
Laramie, Wyoming 82071
(307) 766-2177, 766-2371

TABLE OF CONTENTS

FIGURES

TABLES

FORWARD

This report summarizes research work performed during the first year of ONR Contract N00014-77-C-0503, Project No. 039-149/5-18-77(471), sponsored by the Office of Naval Research, Metallurgy and Ceramics Program, directed by Dr. Arthur M. Diness. Mr. John B. Patton, Naval Weapons Center, China Lake, California, served as program technical monitor.

Initially the program was granted as a one-year effort, beginning 1 August 1977 and extending through 31 July 1978. Additional tasks and funding have since been granted; the program presently is scheduled to end on 31 July 1980.

All work reported here was performed at the University of Wyoming by Mechanical Engineering personnel. Dr. Donald F. Adams, Professor, and Mr. David E. Walrath, Staff Scientist, served as co-principal investigators, assisted by graduate and undergraduate Mechanical Engineering students.

ABSTRACT

A 100 mm (4in) cubic billet of 3-dimensional cartesian weave carbon-carbon material was received in late December, 1977. A series of tests were performed to measure mechanical properties during uniaxial tension, compression, and shear loading. Extensive test development was required as standard tests for these materials do not exist. Strain gages and extensometers were used to measure strain during loading for determination of elastic coefficients. Acoustic emission measurements were performed on selected tests to determine damage thresholds. Failure surfaces were examined in a scanning electron microscope to study failure modes.

SECTION 1

Introduction and Summary

Three-dimensionally reinforced carbon-carbon composites are attracting attention for use in various high temperature, high performance applications, as in rocket nozzle throat regions or re-entry vehicle nose tips. Because this material is a fiber-reinforced composite, its mechanical properties can be tailored by selectively reinforcing specific directions to provide desired strengths and stiffnesses. This ability to control mechanical properties, coupled with favorable ablation, thermal shock, and chemical resistance has prompted interest in acquiring a better understanding of these composite materials.

The intent of this program was to measure the mechanical properties of a specific orthogonally woven 3-D carbon-carbon material, including determination of strengths and elastic coefficients for all three coordinate directions. In addition, an effort was made to determine the onset of irreversible damage to the composite structure due to loading, and to understand the mode of failure taking place. In order to accomplish these goals, specimens were cut from a 100 mm (4 in.) cube of carbon-carbon material supplied by ONR. Tension, compression, and shear tests were performed on specimens oriented parallel to each of the three coordinate directions. As standard test specimen configurations do not exist for this material, several tensile specimen configurations were tried, with only moderate success. Problems arose due to the very low shear strength of this material as compared to its tensile strength. Compression tests were also only partially successful as a great deal of fiber buckling and crushing took place at the specimen ends. One of

the most encouraging aspects of the program was the development of the Iosipescu shear test for use with carbon-carbon composites. Specimens were simple and inexpensive to fabricate, the method was easy to apply, and the results were both repeatable and consistent with results of other investigators using different test methods.

Strain gages did not work at all well in testing any of the carbon-carbon specimens. The material is locally so nonhomogeneous that a small strain gage is only partially strained depending on whether it is attached to fiber bundles or matrix material. Larger strain gages would help "average" out the effects of local nonhomogeneity, but could not be applied to the smaller test specimens. An effort was made to minimize specimen size due to the expense and limited availablility of material.

In order to determine the damage thresholds under various loadings, acoustic emission was monitored during testing. Results of these tests indicate significant irreversible changes do take place within the composite structure well before specimen failure. A limited number of test specimens were loaded just past this threshold point, then sectioned and examined with the scanning electron microscope to detect and identify the damage mode taking place. Both failed and untested specimens were also examined.

This report has been divided into four sections, including this introduction. Section 2 deals with test methodology and results, Section 3 with failure mode detection and identification, and Section 4 summarizes the conclusions of this first-year effort.

SECTION 2

Mechanical Properties Measurements

2.1 Material

Two orthogonal weave carbon-carbon billets were manufactured for ONR by Fiber Materials, Incorporated, Biddeford, Maine. Each billet was approximately 200 mm x 100 mm x 100 mm (8in x 4 in x 4 in), with an average density of 1.9 g/cm^3. Specimens tested during this program were cut from Billet Number 2696; this billet is shown in Figure 1. HM-3000 graphite yarn was used to weave the billet preform. Fiber bundles oriented parallel to the long axis of the billet, designated the z coordinate axis, contained 15,000 filaments per bundle, with bundles spaced 1.57 mm (0.062 in) apart. Fiber bundles oriented in the x and y coordinate directions contained 6000 filaments per bundle, and bundles were spaced 1.42 mm (0.056 in) apart[1].

The University of Wyoming received one-half of Billet Number 2696, a 100 mm (4 in) cube. The remaining half was tested at Southwest Research Institute, San Antonio, Texas. The Wyoming cube was cut into tension, compression, and shear specimens, oriented to measure mechanical properties in all three of the principal material coordinate directions. All cutting was performed at the University of Wyoming using a wire saw. This saw uses a small diameter metal wire imbedded with diamonds, to make very narrow kerf width cuts; a 0.2 mm (0.008 in) diameter wire was used to cut the carbon-carbon, as shown in Figure 2. This cutting method was used to minimize material waste, not because carbon-carbon is difficult to machine.

2.2 Tension Testing

2.2.1 Specimen Configuration

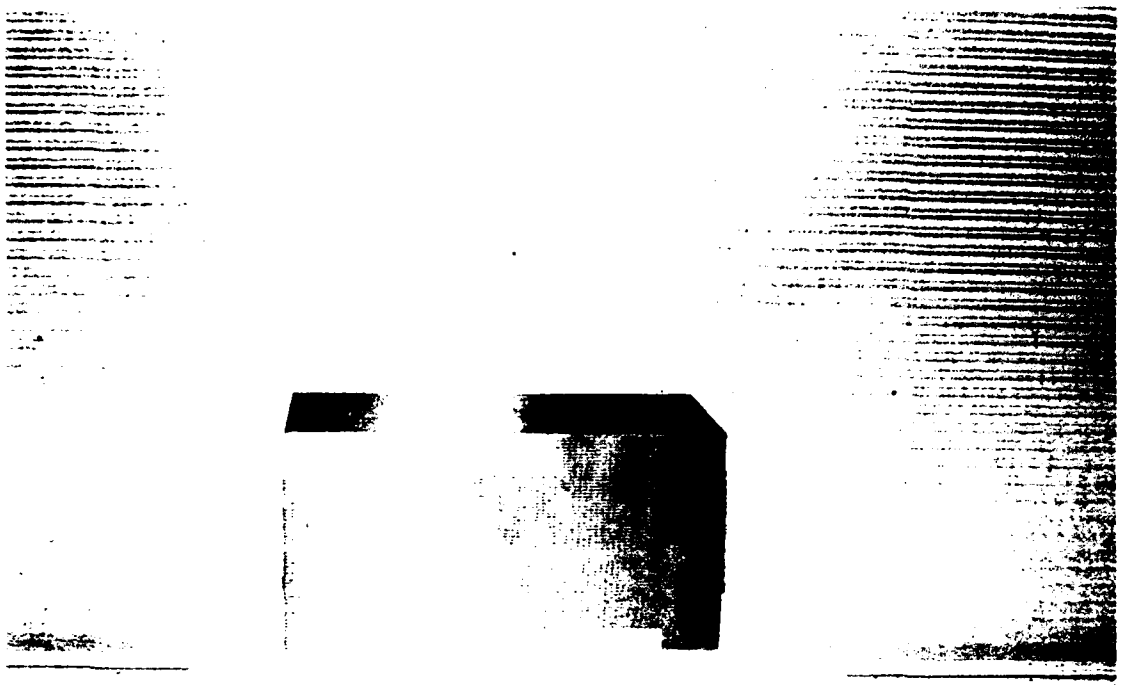

FIGURE 1

ORTHOGONAL WEAVE CARBON-CARBON COMPOSITE BILLET BEFORE CUTTING

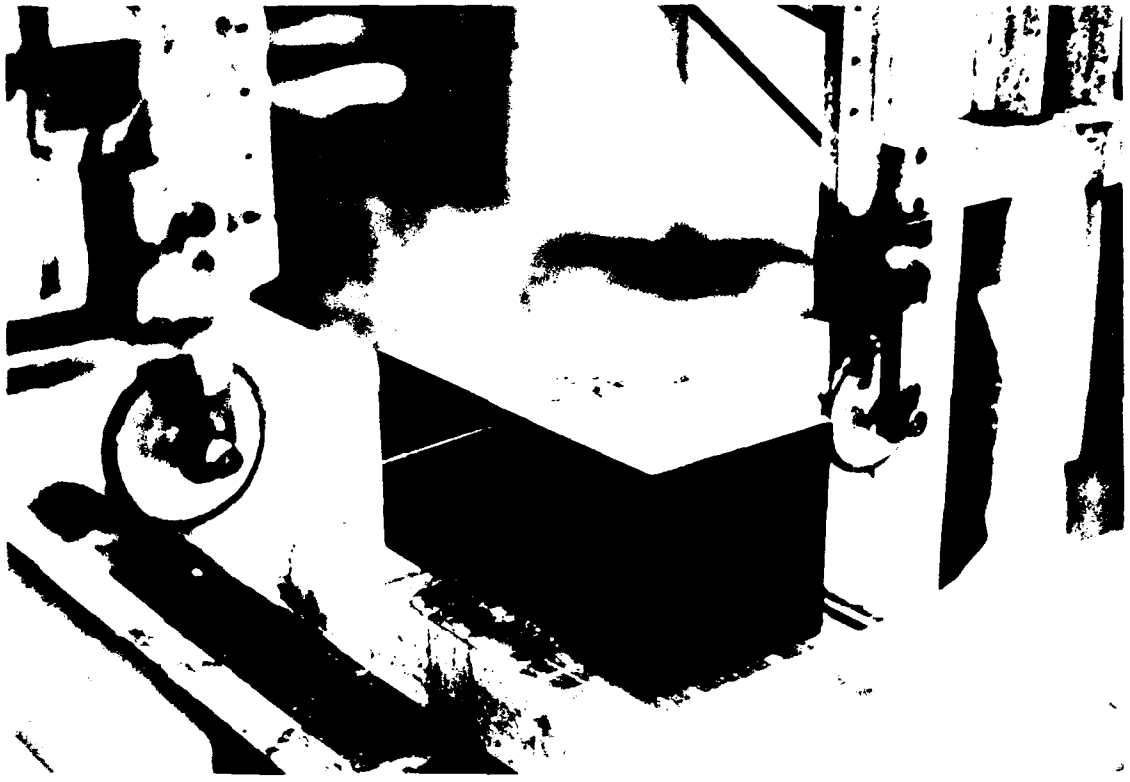

FIGURE 2

CUTTING THE CARBON-CARBON BILLET IN THE WIRE SAW

One of the major problems encountered during the program was designing a suitable tensile specimen configuration. Two factors were considered in designing these specimens. First, carbon-carbon is not at all locally homogeneous. Fiber bundle spacing for this material was on the order of 1.42 to 1.57 mm (0.056 to 0.062 in). Therefore, a tensile specimen required a large cross-sectional area to average out local inhomogeneities, thus avoiding tensile tests on single or small numbers of fiber bundles. The second factor to be considered was the limited amount of available material, a 100 mm (4 in) cube.

A total of four different tensile test specimen configurations were tried during a series of 42 individual tensile tests. The initial specimen configuration was a 100 mm (4 in) long rectangular prism with a square cross section. These specimens were cut such that they contained 36 fiber bundles in a 6 x 6 array across the cross-sectional area. Fiberglass/epoxy tabs were bonded to the end 25 mm (1 in) on all four sides as shown in Figure 3. These tabs were 50 mm (2 in) in length, with a 6 mm (0.25 in) hole to accommodate a pin-clevis grip arrangement. An epoxy adhesive was used to bond these tabs to the specimen, and to fill the 25 mm (1 in) long cavity at the end of the specimen formed by the extra tab length. This specimen configuration was not successful as the carbon-carbon material simply pulled out of the tabs during initial tests.

To increase the shear area within the tabs, the length of each specimen end covered by tabs was increased to 38 mm (1.5 in), thus leaving only a 25 mm (1 in) gage section. When tested, these specimens also tended to fail in the tab region, stripping the tab away from the carbon-carbon test piece.

In an effort to further increase the shear transfer of the adhesive bond, small grooves were cut into the carbon-carbon specimens to establish a mechanical bonding between the test specimen and the adhesive. However, when

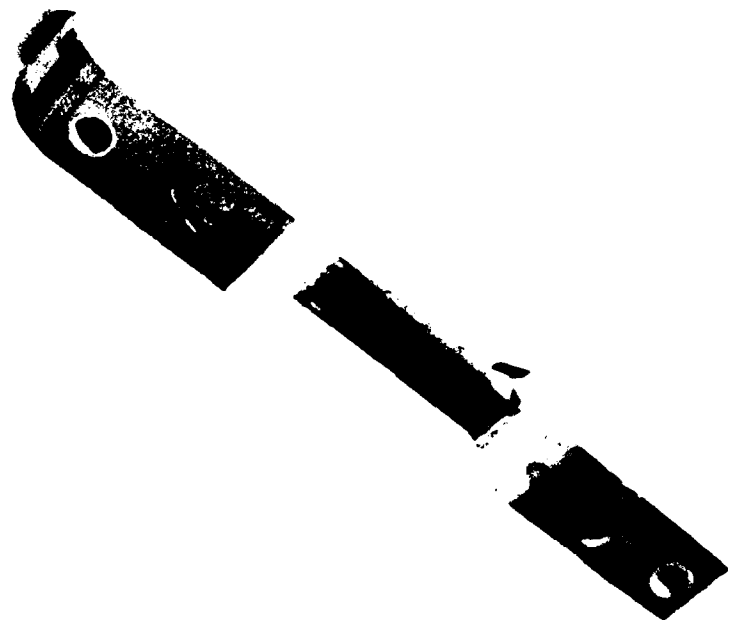

FIGURE 3

EXAMPLE CARBON-CARBON TENSILE SPECIMEN

tested, these specimens also failed in the tabs. It should be noted here that specimens which pulled out of the tabs were retabbed and tested again if no visual evidence of damage was present. This procedure was necessitated by the shortage of material.

The final change in specimen shape was to neck down the gage section of the specimen to decrease the required load at the tabs for a given failure strength. This step was left as a last resort to enable testing of as large a cross section as possible. With 100 mm (4 in) long specimens, a 36 fiber bundle (6 x 6 array) cross section just could not be loaded to cause failure in the gage section; therefore, the cross section was reduced to a 6 x 4 array of fiber bundles. Specimens oriented parallel to the x and y coordinate directions did then fail in the gage section approximately 50 percent of the time. A successful test is shown in Figure 4; a tab failure is shown in Figure 5. No gage section failures were obtained for the stronger z-direction specimens even when the cross-sectional array of fiber bundles was reduced to 5 x 2. Failures of z direction tensile specimens tended to occur by fiber pullout, an extreme example of which is shown in Figure 6.

Tensile specimens were instrumented with strain gages to measure both longitudinal and lateral strains, in order to calculate the elastic coefficients. Gage grids 3.2 mm (0.125 in) square were used; overall strain gage size was 0.25 in. Strain gage behavior was greatly affected by the composition of the surface on which the gages were bonded, as was to be expected with such an inhomogeneous material. An effort was made to bond the strain gages to fiber bundles if possible rather than to a layer of matrix material. Extensometers were also employed to measure longitudinal strains, as a check of the strain gage measurements.

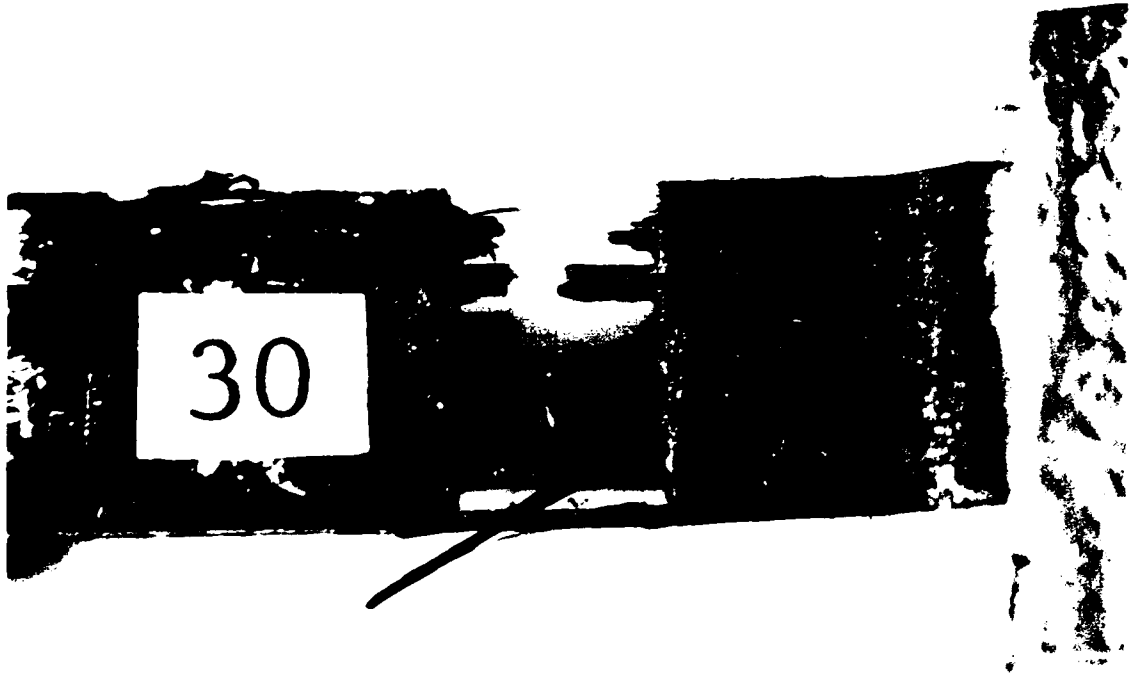

FIGURE 4

EXAMPLE GAGE LENGTH FAILURE OF A TENSILE SPECIMEN

FIGURE 5

EXAMPLE TAB AREA FAILURE OF A TENSILE SPECIMEN

FIGURE 6

FIBER BUNDLE PULL-OUT OF A Z-DIRECTION TENSILE SPECIMEN

Acoustic emission sensors were placed on selected tensile specimens to monitor acoustic activity throughout a test. This was done in an effort to pinpoint the stress at which irreversible damage began to take place within the material. Acoustic emission results will be discussed in Section 3. All data were recorded on a Hewlett-Packard 2100-S minicomputer data acquisition system for later processing and plotting.

2.2.3 Results

A total of 42 tensile tests were performed on 24 individual test specimens. As was previously mentioned, specimens which pulled out of their tabs during testing were retabbed and retested, some as many as four times. Although this retesting procedure is not normally desirable, it was forced by lack of sufficient material.

Results for the tensile tests are summarized in Tables 1 through 3 for the three coordinate directions. The tables are organized such that all of the attempted tests for a given specimen are shown. The last entry for each specimen is the test which finally destroyed the sample. Maximum stresses listed are the maximum tensile stresses attained during the test. All elastic parameters were not measured for each test, or meaningful values could not be calculated due to extreme noise within the data; these conditions are noted in the tables. Although an attempt was made to measure lateral strain, results were too scattered to calculate meaningful Poisson's ratio values. Thus, these elastic coefficients are not included in the tables. This inability to accurately measure the lateral strains stems mainly from the inhomogeneity of the material. Lateral strain magnitudes were less than the axial strain values, and therefore more difficult to measure accurately. Measurement of smaller strains, coupled with inhomogeneous surfaces and small

TABLE 1

TENSILE TEST RESULTS FOR x-AXIS SPECIMENS

Specimen Number	Average Elastic Modulus (GPa)	(Msi)	Maximum Stress (MPa)	(ksi)	Failure Type
XT1	31*	4.5*	119	17.3	T
XT2	50	7.3	101	14.6*	T
XT3	43	6.2	52**	7.6**	T
	48	7.0	102**	14.8**	T
	49	7.1	110**	16.0**	T
	43	6.2	118	17.1	T
XT4	53	7.7	108**	15.6**	T
	54	7.9	102*	14.8*	T
XT5	34	5.0	136	19.7	G
XT6	32*	4.6*	135	19.6	G
XT7	--	--	129	18.7	T
XT8	61	8.8	128	18.5	G
XT9	35	5.1	102*	14.8*	G
Average	47	6.8	128	18.5	
Standard Deviation	8	1.2	8	1.1	

* - not included in the average
** - only final failure strengths are included in the average

-- - bad data

T - tab failure
G - gage length failure

TABLE 2

TENSILE TEST RESULTS FOR y-AXIS SPECIMENS

Specimen Number	Average Elastic Modulus (GPa)	(Msi)	Maximum Stress (MPa)	(ksi)	Failure Type
YT1	56	8.2	104**	15.1**	
	60	8.7	117**	17.0**	
	50	7.3	98**	14.2**	
	43	6.2	101*	14.6*	T
YT2		--	148	21.4	T
YT3	53	7.7	110**	16.0**	
	56	8.1	146	21.2	G
YT4	44	6.4	153	22.2	T
YT5	26*	3.8*	128	18.6	T
YT6	60	8.7	84**	12.2**	
	60	8.7	85**	12.3**	
	57	8.2	128	18.5	T
YT7	63	9.1	154	22.4	P
Average	54	7.9	143	20.7	
Standard Deviation	7	1.0	12	1.7	

* - not included in the average
** - only final failure strengths included in the average

-- - bad data

T - tab failure
G - gage length failure
P - fiber bundle pullout

TABLE 3

TENSILE TEST RESULTS FOR z-AXIS SPECIMENS

Specimen Number	Average Elastic Modulus (GPa)	(Msi)	Maximum Stress (MPa)	(ksi)	Failure Type
ZT1		--	115**	16.7**	T
	108	15.6	123**	17.8**	T
		--	168**	24.3**	T
		--	172	24.9	T,P
ZT2	128	18.6	119*	17.2*	T
ZT3	105	15.2*	183	26.6	T,P
ZT4		--	148	21.5	T
ZT5	148	21.5	139**	20.2**	T
			142	20.6	T
ZT6	115	16.7	180	26.1	T
ZT7	118	17.1	150	21.8	T
ZT8	129	18.7	113**	16.4**	T
	108	15.6	123**	17.8**	T
	129	18.7	122**	17.7**	T
		--	202**	29.3**	T
		--	236	34.2*	T
Average	123	17.8	163	23.6	
Standard Deviation	14	2.0	18	2.6	

* - not included in the average
** - only final failure strengths included in the average

-- - bad data

T - tab failure
G - gage length failure
P - fiber bundle pullout

strain gage size produced erratic results. Extensometers should be much more effective for measuring strains, both lateral and axial, in future work.

Average strength and elastic modulus values have been calculated for each of the three coordinate directions. Average strength values include only final strengths from tests which destroyed the specimen. Modulus values from all tests were included in the averaging process. Values of strength (or elastic modulus) which fell outside the range of plus or minus one standard deviation from the first average were eliminated from the process and a second average was calculated. Eliminated values are denoted by one asterisk. This elimination was performed only once. Therefore, values may be included in the second average which are outside the range of plus or minus one standard deviation as determined the second time. As can be seen in the data, x and y direction mechanical properties are similar as would be expected due to similar fiber contents. The z direction fiber content was higher; therefore, these mechanical properties should be greater than those in the x or y directions.

As was previously mentioned, z direction fiber bundles were spaced 1.57 mm (0.622 in) apart, while the x and y direction fiber bundles were spaced 1.42 mm (0.056 in) apart. The unit cell dimensions are therefore 1.57 x 1.57 x 1.42 mm (0.062 in x 0.062 in x 0.056 in) as shown in Figure 7. An estimate of the reinforcement in the composite is the number of fibers per unit cross-sectional area of the unit cell. For z direction bundles, the cross-sectional area of the unit cell is 1.57 x 1.57 = 2.46 mm^2. The corresponding area for x and y direction bundles is 1.57 x 1.42 = 2.23 mm^2. The reinforcement per unit area for the z direction is then 15,000/2.46 = 6098 filaments/mm^2, and 6000/2.23 = 2691 filaments/mm^2 for the x and y directions. If it is assumed that the matrix material adds little to the tensile strength and stiffness, then the z direction tensile properties should be 6098/2691 = 2.27 times greater

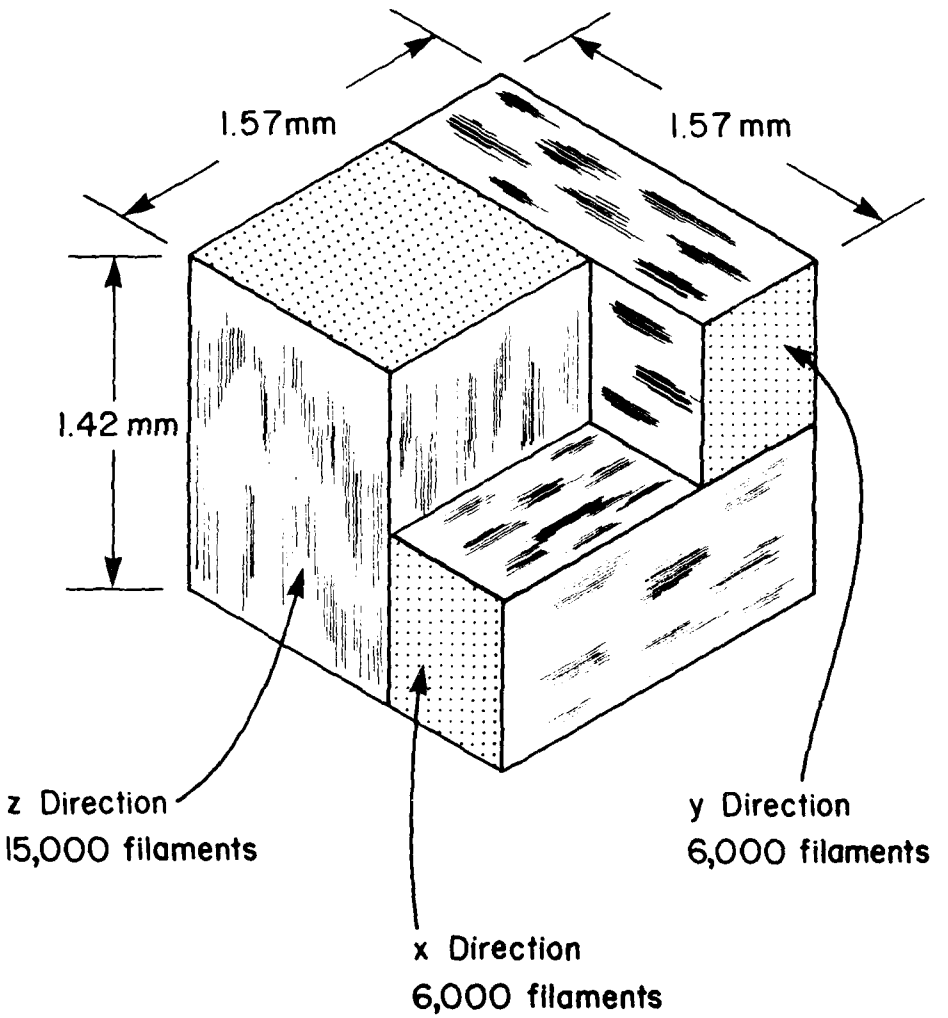

FIGURE 7

UNIT CELL DIMENSIONS FOR THE CARBON-CARBON COMPOSITE MATERIAL TESTED

than the x or y direction tensile properties. From the data of Tables 1 through 3 it can be readily seen that the z direction strengths are nowhere near 2.7 times greater than the x and y direction tensile strengths. However, no reliable z direction tensile strengths were obtained as all failures occurred in the tab regions of the specimens.

The average elastic modulus in the z direction is 2.62 times that in the x direction and 2.28 times that in the y direction, near the ratio of 2.27 predicted. This could indicate a true z direction tensile strength of approximately 327 MP_a (47 ksi) is possible. As a rough first approach, the reinforcement per unit cell area may be used to predict tensile mechanical property ratios.

2.3 Compression Testing

2.3.1 Specimen Configuration

Compression specimens tested during this program were 25 mm (1 in) long with a 12 mm (0.5 in) cross section. End edges were beveled in an attempt to reduce brooming of the ends during loading. A typical compression specimen is shown in Figure 8.

2.6 Compression Testing - Instrumentation

Strain gages were used to measure specimen deformations during compression loading. As in instrumentation of the tensile specimens, an effort was made to bond the strain gages to fiber bundle surfaces rather than to matrix material. Both longitudinal and lateral gages were installed in order to measure both elastic moduli and Poisson expansions. Due to the limited size of the specimens, no extensometers were used; however, loading platen movement was recorded. Acoustic emission transducers were not used, again due to space constraints.

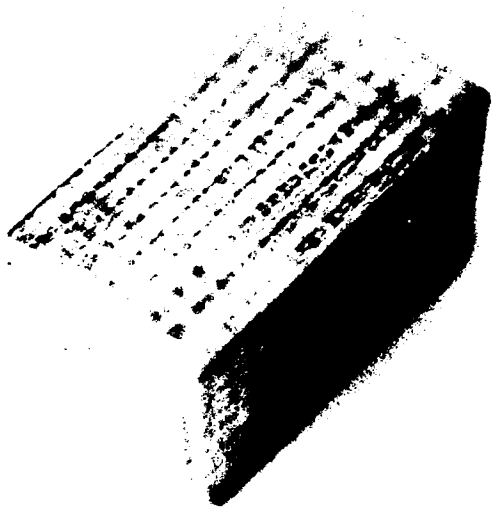

FIGURE 8

EXAMPLE CARBON-CARBON COMPRESSION SPECIMEN

2.3.2 Results

Results of the compression tests for all three coordinate directions are shown in Table 4. Twelve room temperature compression tests were performed, with at least three tests in each of the three coordinate directions. As in the tensile tests, lateral strains were measured, but results were too scattered to obtain meaningful Poisson's coefficient values. Elastic moduli were calculated from the longitudinal strain readings, however.

All compression specimens failed at the loading surfaces, by crushing outward similar to the failed specimen shown in Figure 9. As these failures did not occur in the gage section, the recorded strength values are probably lower than the true material strengths. This also would account for the similarity between x, y and z direction compression strength values. Compression moduli for the z direction specimens are greater than those for x and y direction specimens. Too few modulus results were obtained for y and z direction specimens to obtain good statistical results.

2.4 Shear Testing

2.4.1 Specimen Configuration

A relatively new shear test, the Iosipescu shear test method, was used to obtain the shear properties reported here. This test method was first introduced by Nicolae Iosipescu of Bucharest, Romania, in the early 1960's. Several papers were published (in Romanian) in Romanian journals during the 1963-1965 time period, describing the test. In 1967, Iosipescu published a paper in the ASTM Journal of Materials [2]. This method was brought to the present authors' attention by Mr. Thomas Place of the Aeronutronic Division, Ford Aerospace & Communications Corporation, Newport Beach, California, where it was being used to test three-dimensionally reinforced ceramic matrix materials.

TABLE 4

COMPRESSION TEST RESULTS

Specimen Number	Orientation	Average Elastic Modulus (GPa)	(Msi)	Strength (MPa)	(ksi)
XC1	x	72	10.4	79	11.5
XC2		68	9.8	72	10.4
XC3		54*	7.9*	100	14.5
XC4		64	9.3	98	14.2
Average		68	9.8	88	12.7
Standard Deviation		4	0.6	14	2.0
YC1	y	79	11.4	80	11.6
YC2		--	--	75	10.9
YC3		98	14.2	86	12.5
Average		88	12.8	81	11.7
Standard Deviation				6	0.8
ZC1	z	161	23.3	97	14.0
ZC2		118	17.1	91	13.2
ZC3		--	--	94	13.7
ZC4		--	--	83	12.1
ZC5		--	--	82	11.9
Average		139	20.2	90	13.0
Standard Deviation				6	0.9

* - not included in the average

-- - bad data

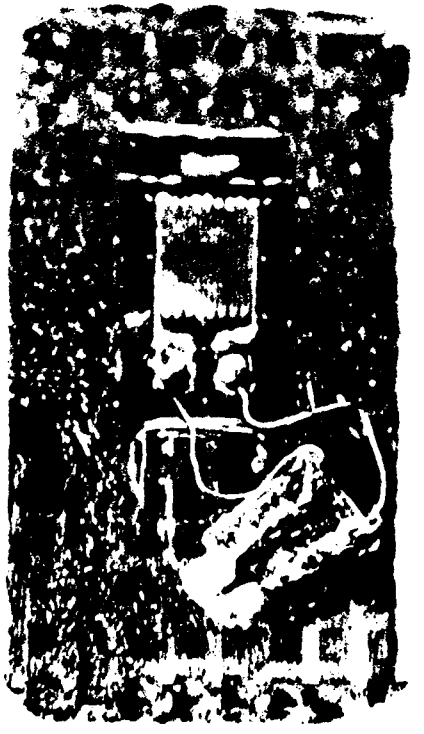

FIGURE 9

TYPICAL FAILURE OF COMPRESSION SPECIMENS

Specimens tested in this program were 51 mm (2 in) long, 12.7 mm (0.50 in) tall, and 10 mm (0.40 in) thick; a sample is shown in Figure 10. Load is applied as two opposing moments, as shown in Figure 11, which cancel at the center plane of the specimen to produce a state of pure shear. The loading fixture which was built for this program is shown in Figure 12.

2.4.2 Instrumentation

All shear specimens were instrumented with two strain gages oriented at 45° and centered on the shear line. Due to limited space in the gage section, no acoustic emission measurements were taken. Loading head position was also monitored throughout the tests.

2.4.3 Results

Shear strength and modulus data are presented in Table 5 for the three coordinate directions. A total of 13 shear tests were performed on three shear planes. Load was applied parallel to the second coordinate mentioned; for example, an xz specimen was sheared on the yz plane with load applied parallel to the z direction. The x coordinate direction would then correspond to the long axis of the specimen, perpendicular to the shear plane.

Shear strengths appear to be quite consistent, as indicated by the low standard deviation values for the three sets of specimens. Little difference in strength was noted between the three different shear planes. The shear strength for this carbon-carbon material was about 16 MPa, independent of the fiber bundle plane being sheared. Shear modulus results are somewhat more scattered but again very little difference exists in the values for the three different shear planes. Scatter in strain data was due to problems with strain gages on this inhomogeneous material. Experiments are currently being continued,

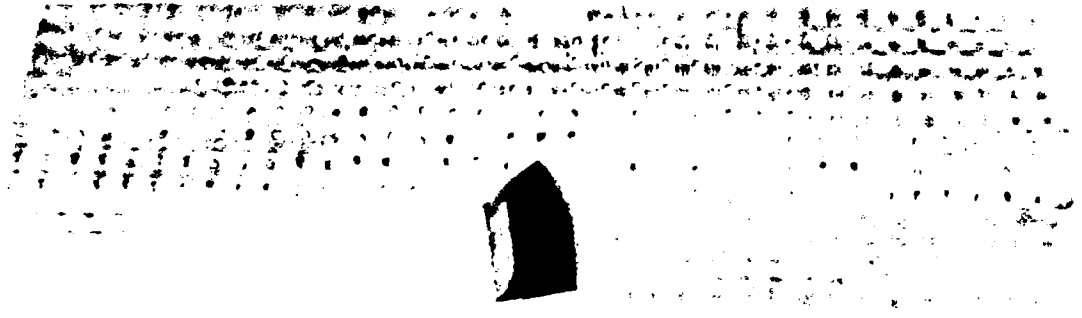

FIGURE 10

EXAMPLE CARBON-CARBON IOSIPESCU SHEAR SPECIMEN

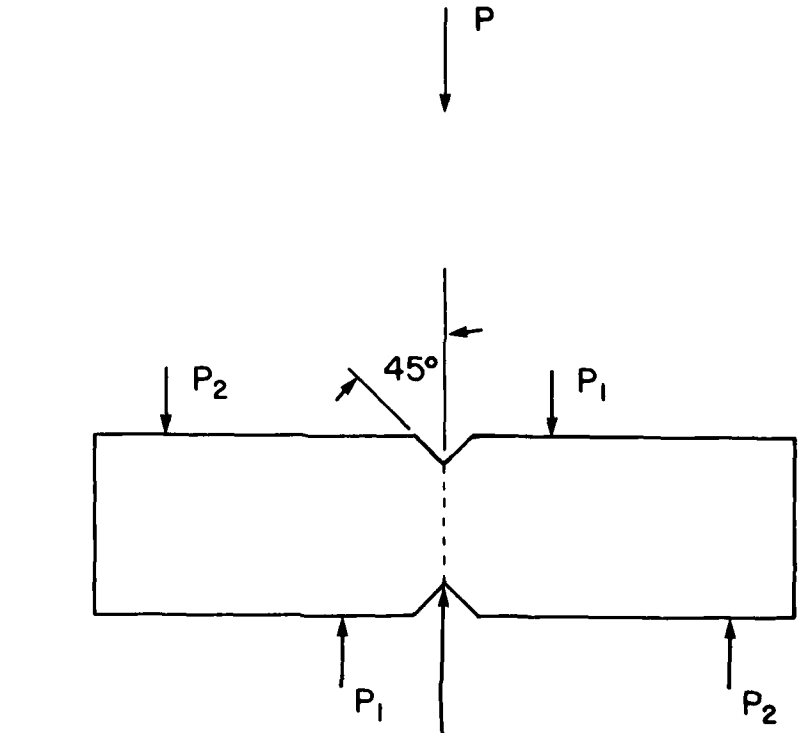

FIGURE 11

LOADING IN THE IOSIPESCU SHEAR TEST

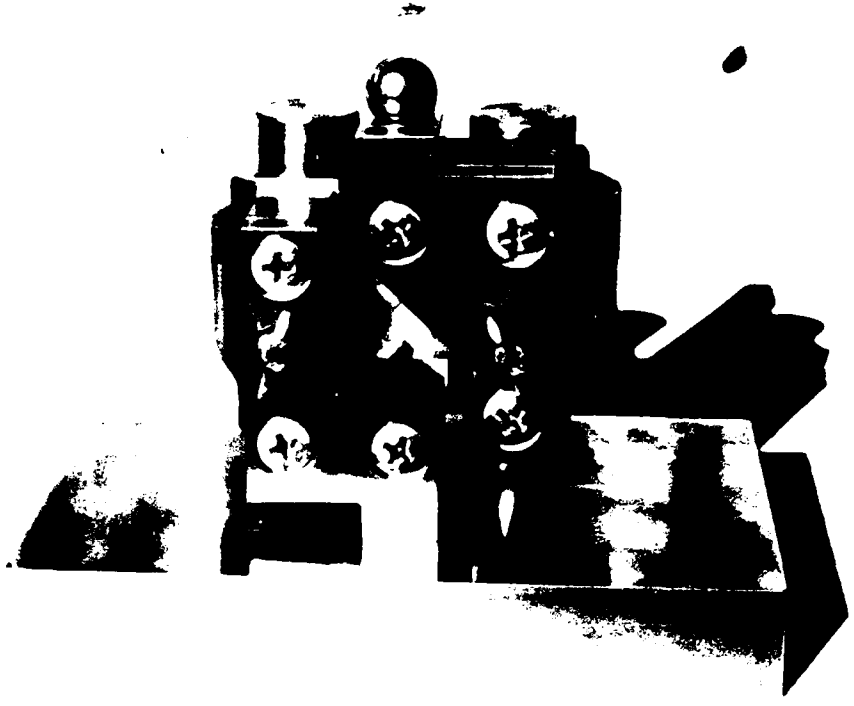

FIGURE 12

IOSIPESCU SHEAR TEST FIXTURE

TABLE 5

IOSIPESCU SHEAR TEST RESULTS

Specimen Number	Shear Plane*	Shear Modulus (GPa)	(Msi)	Shear Strength (MPa)	(ksi)
XZ1	xz	2.1	0.31	15	2.1
XZ2		3.2	0.46	14	2.0
XZ3		1.4	0.20	17	2.5
XZ4		2.1	0.31	16	2.3
XZ5		1.0**	0.15**	18	2.6
Average		2.2	0.32	16	2.3
Standard Deviation		0.8	0.11	2	0.3
YX1	yx	2.5	0.36	15	2.2
YX2		1.0**	0.15**	15	2.2
YX3		1.4	0.20	14	2.0
YX4		--	--	17	2.4
Average		1.9	0.28	15	2.2
Standard Deviation				1	0.2
ZY1	zy	2.6	0.37	19	2.7
ZY2		2.6	0.37	17	2.4
ZY3		3.4	0.50	17	2.4
ZY4		1.9	0.28	16	2.3
Average		2.6	0.38	17	2.4
Standard Deviation		0.6	0.09	1	0.2

* - xz plane, load was applied perpendicular to x, parallel to z, etc.
** - not included in the average

-- - bad data

using the fixture displacement values in making the shear strain calculations, to avoid using strain gages.

SECTION 3

Identification Of Damage Initiation And Failure Modes

3.1 Acoustic Emission

Acoustic emission was monitored during 14 tensile tests, using two transducers with resonant frequencies of 230 kHz. The cumulative count of acoustic emission events was recorded throughout each test. Due to limited specimen surface area on shear and compression specimens, acoustic emission was monitored during tensile tests only.

Data processing consisted of plotting stress versus cumulative acoustic emission and stress versus strain on one plot for each specimen. An example of such a plot is shown in Figure 13. Cumulative acoustic emission event count is plotted along the x-axis, with stress plotted on the y-axis. Superimposed on this is the stress-strain curve recorded for this test. As can be seen in the curves, little acoustic activity took place until a stress level of about 97 MPa (14 ksi) was reached. At this stress level, significant acoustic activity took place, followed by a "quiet" period as stress increased. Acoustic emissions began to reoccur as ultimate stress was approached, with a great deal of activity occurring just before and during specimen failure. Notice, however, no irregularities are present in the stress-strain curve during high acoustic emission activity. Plots for the other 13 specimens were very similar to the plot shown in Figure 13. If an acoustic threshold stress is defined as the stress at which significant activity begins, then the threshold stress for the test shown in Figure 13 is about 97 MPa. Threshold stresses and ultimate strengths for this test and the other acoustically monitored tests are listed in Table 6. As can be seen from these data, significant acoustic activity was apparent well before actual specimen failure. Acoustic thresholds ranged from 30 to 75 percent of ultimate failure stresses.

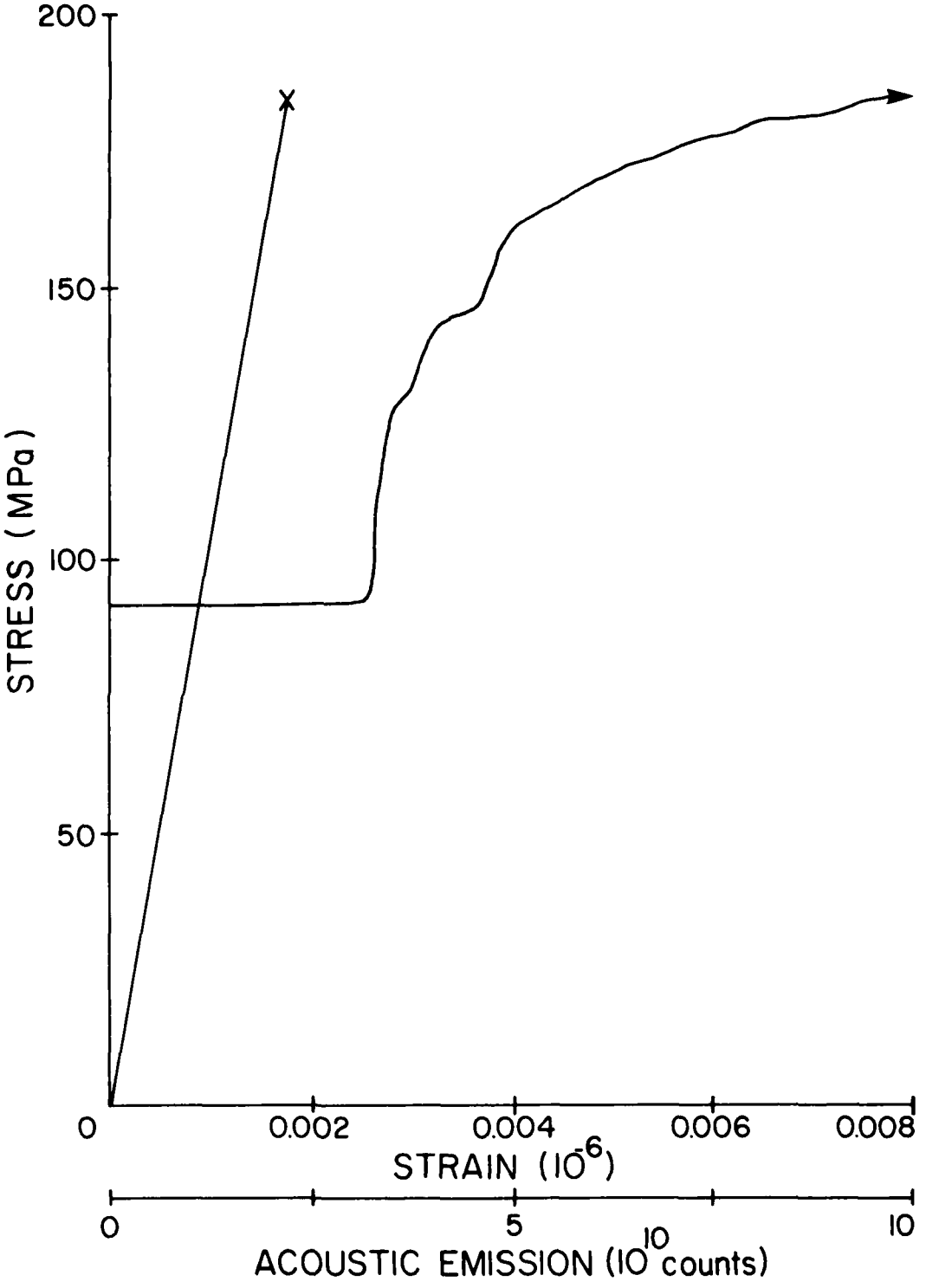

FIGURE 13

EXAMPLE STRESS-STRAIN AND ACOUSTIC EMISSION PLOT

TABLE 6

DAMAGE INITIATION DETERMINED BY ACOUSTIC EMISSION DURING TENSILE TESTS

Specimen Number	Orientation	Threshold Stress (MPa)	(ksi)	Ultimate Stress (MPa)	(ksi)
XT1	x	69	10	119	17.3
XT2		76	11	101	14.6
XT5		41	6	136	19.7
XT6		48	7	135	19.6
XT8		90	13	128	18.5
XT9		34	5	102	14.8
YT4	y	41	6	153	22.2
YT5		48	7	128	18.6
YT7		97	14	154	22.4
ZT3	z	97	14	183	26.6
ZT4		48	7	148	21.5
ZT5		69	10	139	20.2*
ZT5		48	7	142	20.6
ZT6		48	7	180	26.1
ZT7		48	7	150	21.8

* pulled out of tabs during first test

3.2 Tensile Damage Thresholds

Acoustic emission was monitored in an effort to determine at what point in the loading of a specimen that irreversible damage occurred within the material. To identify this damage, specimens were loaded past their individual acoustic thresholds but not to failure. These specimens were then sectioned and examined with the scanning electron microscope (SEM). For comparison, sections were examined from material which had never been loaded.

A SEM photograph of nonloaded carbon-carbon is shown in Figure 14. Magnification in this photograph is 100X. Fiber bundles are present along the right side and along the bottom of the picture. These fibers are parallel to the plane of the page at the bottom edge, and perpendicular to the page along the right hand side. Notice the cavity formed by the intersecting bundles in the upper left hand corner. The matrix material has contracted to form a sphere which sits in this cavity. These spheres were very loose and tended to fall out if the material was sectioned such that the cavity was opened.

A similar section view of the carbon-carbon is shown in Figure 15. However, this specimen was cut from a partially loaded z direction tensile specimen. This tensile specimen was loaded just past the point at which significant acoustic activity took place, approximately 66.9 MPa (9.7 ksi), then unloaded. A longitudinal section was cut for examination in the SEM. The photograph shown in Figure 15 is a 100X view of the interior of the tensile specimen; loading is along the horizontal axis of the photograph. Notice the crack originating at the unit cell running parallel to the z direction fiber bundle along the bottom of the picture. This cracking could be the source of the initial acoustic activity and is evidence that material damage occurs well before ultimate failure.

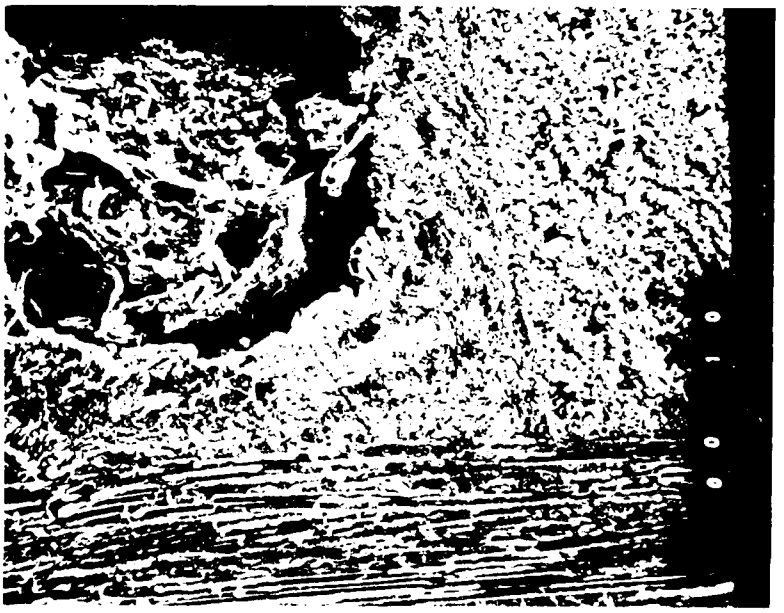

FIGURE 14

NONLOADED CARBON-CARBON, 100X

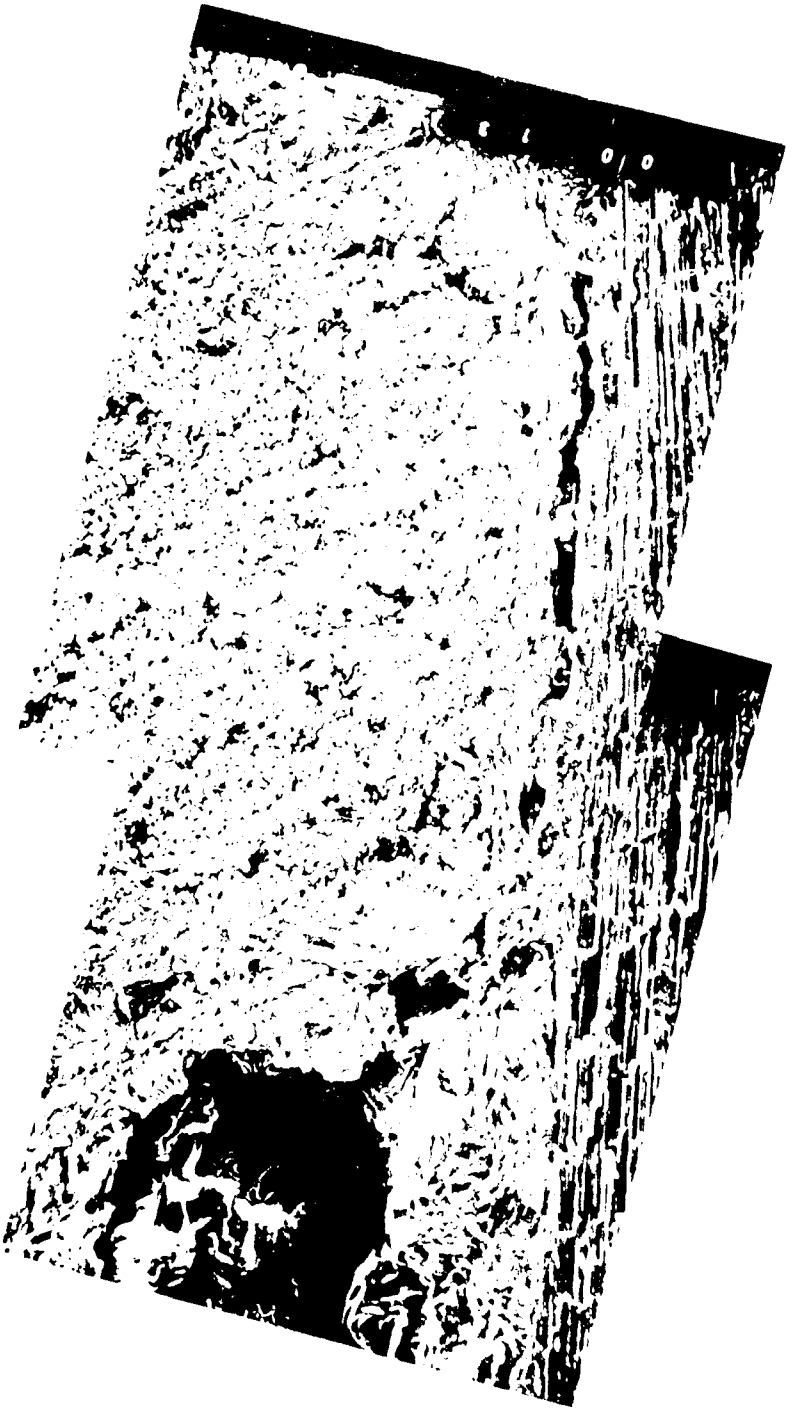

FIGURE 15

CRACK IN PARTIALLY LOADED Z DIRECTION TENSILE SPECIMEN, 100X

3.3 Compression Failure Modes

As was previously discussed, all compression failures occurred at or near the loading plattens. No acoustic monitoring was performed during these tests, therefore, no partial loading tests were performed. Failed compression specimens were sectioned and examined in the SEM, however.

Typical compression failures occurred as a result of local fiber microbuckling, as shown in Figure 16. Compression loading was along the vertical axis in this photograph; the magnification is 150X. Fibers buckled locally in bands near the actual transverse fracture plane. Typically, several bands were present near the fracture surface. These photographs of compression failed carbon-carbon are remarkably similar to microphotographs taken at the University of Wyoming, of compression failed graphite/epoxy [3]. Although the matrix material is very different between carbon-carbon and graphite/epoxy, the compression failure mechanisms are the same.

3.4 Shear Failure Modes

Failed shear specimens were also examined with the SEM. A typical failure of an Iosipescu shear specimen is shown in Figure 17, at a magnification of 150X. Shear loading for this specimen was on a plane perpendicular to the page, parallel with the vertical axis of the photograph. The view shown in Figure 17 is on an internal plane; the specimen was sectioned along the longitudinal axis. Two cracks are present, parallel to each other. The first and most prominent is in the left one-third of the photograph while the second, smaller crack is near the right hand edge. Several cracks similar to these were typically found near the center section of each of the Iosipescu shear specimens.

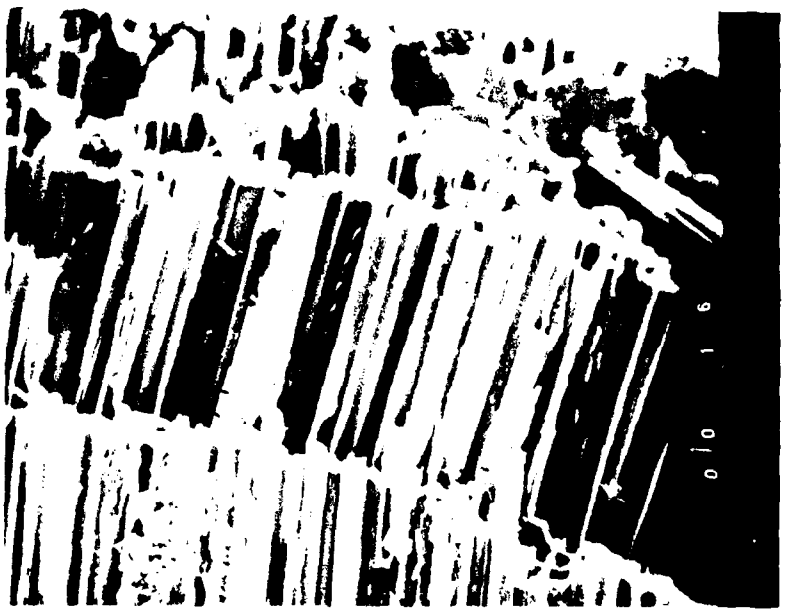

FIGURE 16

COMPRESSION BUCKLING OF Z DIRECTION FIBERS, 150X

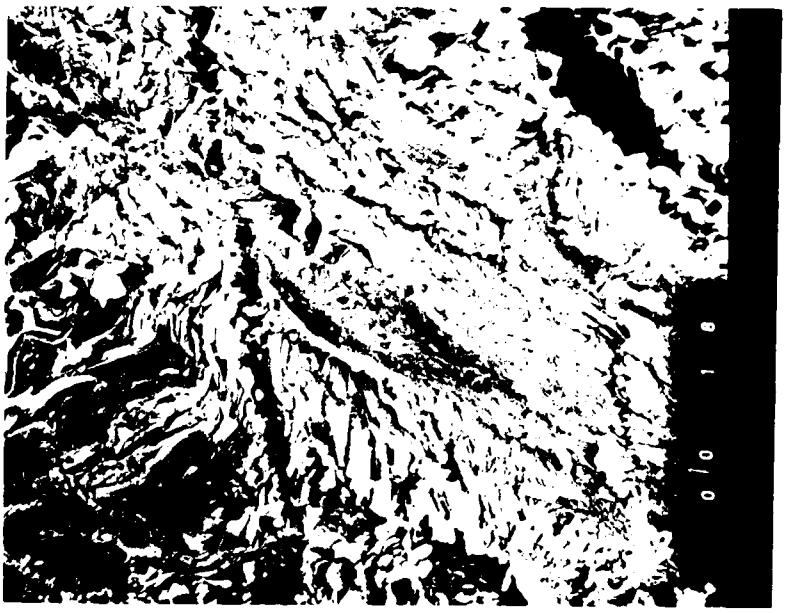

FIGURE 17

SHEAR CRACK IN A YX IOSIPESCU SHEAR SPECIMEN, 150X

As a check on the validity of the shear strength values, three compression tests were performed on specimens whose x and y coordinates were oriented at 45 degrees to the loading direction. Compressive load was thus applied parallel to the z axis, at an angle with the x and y axes. Failure strengths for these three tests are listed in Table 7. Notice the values compare closely with the shear strengths listed in Table 5. Examination of sectioned failed specimens revealed extensive cracking present parallel to the x and y direction fiber bundles. One such crack is shown in Figure 18. This view is looking parallel to the load direction at a cross section cut from the center of the specimen. Notice how the crack proceeds around the fiber bundle. The crack is also quite deep into the specimen; the fiber bundle is essentially loose within the matrix, held in place by loose matrix material, and other fiber bundles.

TABLE 7

COMPRESSION TEST RESULTS FOR 45 DEGREE SPECIMENS

Specimen Number	Compression Stress (MPa)	(ksi)	Shear Stress (MPa)	(ksi)
C41	30.4	4.41	15.2	2.21
C42	31.2	4.53	15.6	2.26
C43	32.1	4.65	16.1	2.33

FIGURE 18

CRACK IN A 45 DEGREE COMPRESSION SPECIMEN, 100X

SECTION 4

Conclusions

The purpose of this program was to characterize a specific orthogonal weave carbon-carbon material. During the course of this first-year effort, a great deal of experience was gained in test methods, specimen design, and instrumentation.

Tensile testing of this material was one of the more difficult problems. Several different versions of a tabbed specimen were tried, with only moderate success. The major difficulty was related to the low shear strength of the material as compared to the tensile strength. Possible solutions to the resulting gripping problem would be to use longer specimens, an option not available during this program because of the size of the billet available, or to try a mechanical gripping arrangement instead of using adhesives. New tensile specimen configurations are being used in the second-year effort.

Compression specimen design was also a problem in this program. Most failures took place at the loading plattens. This problem can be corrected by using a center tapered compression specimen to insure the maximum stress is in the center of the gage section.

The success of the Iosipescu shear test was one of the more encouraging results of the program. Test results were very repeatable and consistent with results from other types of shear tests. The Iosipescu shear test is simple and inexpensive to perform, and should be investigated further for use with other materials.

Strains during most tests were measured with strain gages, a method that was only partially successful. Due to the inhomogeneity of the surface, strain measurements were scattered and of little value where strain magnitudes were small. Large strain gages must be used (not practical on small specimens).

A better way must be found to apply them, or extensometers should be used to measure strains in this material. During the second-year effort, much greater use will be made of extensometers.

Damage initiation and damage modes were identified. Acoustic emission monitoring and SEM examination of partially loaded tensile specimens showed that material damage occurred well before ultimate tensile failure. This damage was separation of fiber bundles from the matrix, indicated by cracks along the fiber bundles in partially loaded tensile specimens.

Compression specimens tended to fail due to microbuckling of the fibers. However, these results are somewhat inconclusive as failures occurred near the loading plattens. Further work in this area is currently in progress.

Failed Iosipescu shear specimens showed cracks in the matrix material at the failure plane. Shear failures tended to occur along the matrix-fiber bundle interface, as would be expected.

Work on the second-year effort has now begun with receipt of the material, a polar weave carbon-carbon ring.

REFERENCES

[1] Manufacturers Preform Data Sheet

[2] N. Iosipescu, "New Accurate Procedure for Single Shear Testing of Metals", Journal of Materials, Vol 2, No. 3, September 1967, pp. 537-566.

[3] G. C. Grimes and D. F. Adams, "Investigation of Compression Fatigue Properties of Advanced Composites", Final Report, Naval Air Systems Command Contract Numbers N00019-77-C-0518 and N00019-77-C-0519, April 1979.

DISTRIBUTION LIST

DOD

Office of the Secretary of Defense
Director of Defense Research and
Engineering
OAD/OS/Mr. B. Barse
OAD/ET/Mr. J. Persh
OAD/SW/Dr. R. Ruffine
Washington, DC 20301

Plastics Technical Evaluation
Center, Building 176
ATTN: Mr. A. Anazione
Department of Defense
Picatinny Arsenal
Dover, NJ 07801

AIR FORCE

Air Force Materials Laboratory
AFML/
CC/Dr. F. Kelley
MB/Mr. J. Kelble
MBC/Dr. R. Craig
MBC/Dr. W. Kessler
MBC/Mr. D. Schmidt
MBM/Dr. N. Pagano
MX/Dr. M. Minges
MXE/Lt. T. Curci
MXE/Capt. E. Heinonen
MXE/Mr. J. Latva
MXE/Mr. G. Ormbrek
MXE/Lt. G. Wendt
LTN/Mr. H. Materne
Wright-Patterson AFB, OH 45433

Air Force Office of Scientific Research
AFOSR/NC/Dr. D. Ulrich
NC/Dr. D. Ball
NC/Dr. W. Walker/Dr. C. Hays
L/COL R. Haffner
Building 410
Bolling AFB, DC 20332

Air Force Rocket Propulsion Laboratory
AFRPL/
MK/Dr. C. Hawk
MKC/Mr. L. Tepe
MKCC/Mr. W. Payne
CA/Mr. R. Weiss
Edwards AFB, CA 93523

Air Force Weapons Laboratory
AFWL/
Lt. Col. D. Ericson
Kirtland AFB, NM 87117

SAMSO/ABRES
ATTN: Lt. Col. J. McCormack
Worldway Postal Center
P. O. Box 92960
Los Angeles, CA 90009

Space and Missile Systems
SAMSO/
MNNR/Capt. T. Brocato
MNPX/Capt. D. Bailey
Norton AFB, CA 92409

ARMY

Army Materials and Mechanics Research
Center
ATTN: AMXMR-H/J. Dignam
Watertown, MA 02172

NAVY

Assistant Secretary of the Navy (R&D)
ATTN: Dr. S. Koslov
Washington, DC 20301

Office of the Chief of Naval Operations
ATTN: Mr. R. Blaise (OP-620E)
Department of the Navy
Washington, DC 20350

Director, Naval Research Laboratory
ATTN: Dr. S. Freiman/Mr. P. Mast
(Code 8434)
Washington, DC 20375

Office of Naval Research
ATTN: Dr. A. Diness (Code 471)
800 North Quincy
Arlington, VA 20305

Commander, Naval Sea Systems Command, HQ.
ATTN: Mr. M. Kinna (SEA-0352)
Dr. J. Huth (SEA-03C)
Mr. G. Sorkin (SEA-035)
Washington, DC 20302

Commander
Naval Surface Weapons Center
ATTN: Mr. R. Edwards/Code WA-43
Mr. R. Feldhuhn/Code WA-43
Dr. W. Lyons/Code WA-07
Mr. C. Rowe/Code WR-31
Mr. J. Vamos
Mr. J. Wagner/Code WA-43
Mr. R. Wilson/Code WR-31
White Oak
Silver Spring, MD 20910

Commander
Naval Weapons Center
ATTN: Mr. J. Patton/Code 3161
Mr. E. Jeter/Code 3162
China Lake, CA 93555

Director
Strategic Systems Project Office (PM-1)
ATTN: Dr. J. Kincaid/SP-20
Dr. H. McMasters/SP-2723
Mr. S. Weinger/SP
Department of the Navy
Washington, DC 20376

Project Manager
Trident Systems Project (CNM-PM 2)
ATTN: Mr. J. Crone/HM-2-001
Department of the Navy
Washington, DC 20360

NASA

NASA, Marshall Space Flight Center
ATTN: Mr. B. Powers, EP 25
Huntsville, AL 35812

DNA

Director, Defense Nuclear Agency
ATTN: Mr. D. Kohler
Mr. J. Moulton
Washington, DC 20305

ERDA

U.S. Energy Research Division
Administration
ATTN: Mr. A. Littman
Nuclear Research and Application Div.
Washington, DC 20331

INDUSTRY (OTHERS)

Acurex/Aerotherm
ATTN: Mr. H. Tong
Mr. R. Manfred
Mr. J. Dodson
Mr. J. Zimmer
485 Clyde Avenue
Mountain View, CA 94042

Aerojet
ATTN: Mr. J. Cauzza
Mr. H. Davis
Mr. M. Clone
Mr. R. Dona
P. O. Box 13400
Sacramento, CA 95813

Aeronutronic-Ford
ATTN: Mr. J. Perry
Ford Road
Newport Beach, CA 92663

Aerospace Corporation
ATTN: Dr. S. Batdorf
Dr. H. Blaes
Dr. S. Brelant
Mr. J. Evangelides
Dr. R. Hallse
Mr. W. Herbig
Dr. R. Meyer
Mr. R. Mortensen
Dr. L. Rubin
P. O. Box 92957
Los Angeles, CA 90009

Atlantic Research Corporation
ATTN: Mr. W. Armour
Mr. J. Baetz
Mr. J. Bird
Mr. R. Brown
5390 Cherokee Avenue
Alexandria, VA 22314

Avco Corporation
ATTN: Mr. B. Benz
Mr. G. Mullen
Mr. A. Traverna
Lowell Industrial Park
Lowell, MA 01851

Avco Corporation
ATTN: Mr. P. Rolincik
201 Lowell Street
Wilmington, MA 01887

Battelle Memorial Institute
ATTN: Mr. W. Chard
505 King Avenue
Columbus, OH 43201

Boeing Company
ATTN: Mr. J. Bedwell
P. O. Box 3996/MS 88-19
Seattle, WA 98124

California Research and Tech., Inc.
ATTN: Dr. K. Kreynenhagen
6269 Dariel Avenue
Woodland Hills, California 91364

Carborundum Company
Graphite Products Division
ATTN: Mr. W. Carlson
2050 Cory Drive
Sanborn, NY 14132

Effects Technology, Inc.
ATTN: Mr. J. Green
Mr. M. Graham
5383 Hollister Avenue
Santa Barbara, CA 93105

Mr. D. Ehrentreis
Dave Ehrentreis Consulting Engr.
5 Horizon Road
Ft. Lee, NJ 07024

Fiber Materials, Inc.
ATTN: Mr. L. McAllister
Biddeford Industrial Park
Biddeford, ME 04005

General Electric Co., RESD
ATTN: Mr. P. Bolinger
Dr. J. Gebhardt
Mr. K. Hall
Mr. D. Lowe
Dr. E. Stover
Mr. W. Reiley
P. O. Box 7560 - Room 2023
Philadelphia, PA 19406

General Electric Co., RESD
ATTN: Mr. A. Levine
3198 Chestnut Street
Philadelphia, PA 19101

Great Lakes Carbon Corporation
ATTN: Mr. W. Benn
299 Park Avenue
New York, NY 10017

Great Lakes Research Corporation
ATTN: Mr. H. Gilliam
P. O. Box 1031
Elizabethton, IN 37643

HAVEG
ATTN: Mr. R. Pegg
Mr. R. Rodriguez
12827 East Imperial Highway
Santa Fe Springs, CA 90670

Hercules Corporation
ATTN: Mr. P. Christensen
Mr. K. Dickerson
Mr. B. McKenzie
P. O. Box 98
Magna, UT 84044

HITCO
ATTN: Mr. L. Dyson
1600 West 135th Street
Gardena, CA 90249

Jet Propulsion Laboratory
ATTN: Mr. N. Kimmel
Pasadena, CA 91103

Kaiser
ATTN: Mr. M. Fischer
Mr. W. Sidney
880 Doolittle Drive
San Leandro, CA 94577

Lawrence Livermore Laboratories
ATTN: Mr. A. Maimoni (L-503)
P. O. Box 808
Livermore, CA 94550

Lockheed Missiles and Space Company
ATTN: Mr. R. Greene
Mr. G. Grunwald
Mr. A. Johnson
Mr. A. Mietz
Dr. M. Steinberg
P. O. Box 504
Sunnyvale, CA 94088

Los Alamos Scientific Laboratory
ATTN: Mr. R. Imprescia
Dr. J. Taylor & C. Stein
University of California
P. O. Box 1663
Los Alamos, NM 87545

Materials Sciences Corporation
ATTN: Dr. S. Chatterjee
Dr. J. Kibler
Dr. B. Rosen
Blue Bell Office Campus
Merion Towle Building
Blue Bell, PA 19422

McDonnell Douglas Astronautics Co.
ATTN: Mr. L. Greszczuk
Mr. J. Jortner
Mr. B. Leonard
Dr. J. Peck
Mr. A. Penton
Mr. R. Seibold
5301 Bolsa Avenue
Huntington Beach, CA 92647

McDonnell Douglas Research Labs.
ATTN: H. Holman
P. O. Box 516
St. Louis, MO 63166

NETCO
ATTN: Mr. W. Pfeifer
Ms. P. Sullivan
Mr. R. Young
110 Pine Avenue, Suite 906
Long Beach, CA 90802

Prototype Development Associates, Inc.
ATTN: Mr. Alexander
Dr. G. Crose
Dr. J. McDonald
Mr. G. Schutzler
1740 Garry Avenue, Suite 201
Santa Ana, CA 92705

Sandia Laboratories
ATTN: Mr. D. Northrup
P. O. Box 5800
Albuquerque, New Mexico 87115

Science Applications, Inc.
ATTN: Mr. F. Clayton
Mr. D. Eitman
Mr. K. Kratsch
Dr. W. Loomis
Mr. J. Pope
Dr. P. Randles
201 West Dyer Road, Unit C
Santa Ana, CA 92707

Southern Research Institute
ATTN: Mr. C. Canada
Mr. H. Littleton
Mr. H. Starrett
Mr. C. Pears
2000 Ninth Avenue, South
Birmingham, AL 35205

Southwest Research Institute
ATTN: Dr. Philip H. Francis
Dr. J. Lankford
P. O. Drawer 28510
San Antonio, TX 78284

Stackpole Fibers Company, Inc.
ATTN: Mr. G. Flemming
Foundry Industrial Park
Lowell, MA 01852

Super-Temp Company
ATTN: Mr. D. Bauer
111205 Norwalk Boulevard
Santa Fe Springs, CA 90670

Systems, Science and Software
ATTN: Mr. C. Emde
Dr. G. Gurtman
P. O. Box 1620
La Jolla, CA 92037

Thiokol
ATTN: Mr. G. Broman
Dr. S. Kulkarni
Mr. A. Canfield
Mr. R. Laramee
Brigham City, UT 84302

TRW Systems Defense Space Systems
ATTN: Dr. W. Kotlensky
Building R-1-Room 2012
One Space Park
Redondo Beach, CA 90278

Union Carbide Corporation
Nuclear Division (Y-12 Plant)
ATTN: Mr. A. Taylor
Dr. G. Weber
P. O. Box Y
Oak Ridge, TN 37839

Union Carbide Corporation
Carbon Products Division
ATTN: Mr. J. Bowman
Dr. J. Criscione
P. O. Box 6116
Cleveland, OH 44101

United Technologies
Chemical Systems Division
ATTN: Mr. R. Ellis
Mr. P. O'Driscoll/Mr. S. Slosarik
P. O. Box 358
Sunnyvale, CA 94088

UNIVERSITIES

Department of Physics and Astronomy
Ball State University
ATTN: Mr. S. Mrozowski
Muncie, IN 47306

Franklin Institute Research Labs.
Physics of Materials Laboratory
Material and Physical Sciences Dept.
ATTN: Mr. J. Meakin, Manager
Benjamin Franklin Parkway
Philadelphia, PA 19103

Applied Physics Laboratory
The Johns Hopkins University
ATTN: Mr. W. Caywood
Johns Hopkins Road
Laurel, MD 20810

Department of Materials Science and Engineering
Massachusetts Institute of Technology
ATTN: Dr. D. Uhlmann
Boston, MA 02139

Massachusetts Institute of Technology
ATTN: Mr. J. May
Dr. J. W. Mar
Boston, MA 02139

Aeronautical Research Associates of Princeton
ATTN: Dr. J. McMonagle
Washington Road
Princeton, NJ 08540

Materials Science Department
Pennsylvania State University
ATTN: Dr. P. Walker
State College, PA 16801

Department of Materials Engineering
Rensselaer Polytechnic Institute
ATTN: Dr. J. Diefendorf
Troy, NY 12181

Southern Methodist University
Civil and Mechanical Engineering Department
ATTN: Dr. R. M. Jones
Dallas, TX 75275

University of California, Los Angeles
School of Engineering and Applied Science
ATTN: Dr. G. Sines
Los Angeles, CA 90024

Department of Mining, Metallurgical and Ceramic Engineering
University of Washington
ATTN: Mr. D. Fischbach
Mr. D. Uptegrove
Seattle, WA 98195

University of Wyoming
Department of Mechanical Engineering
ATTN: Dr. D. Adams
Laramie, WY 82071

University of Southern California
ATTN: Mr. T. Yen
Los Angeles, CA 90007

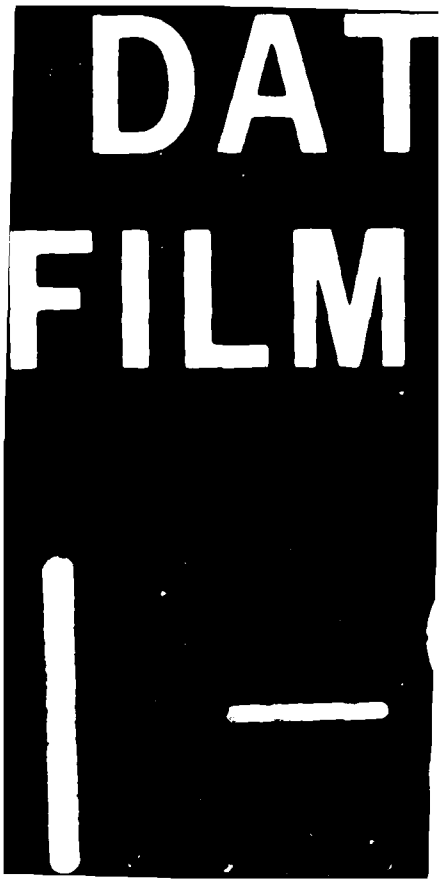
DAT
FILM